RESEARCH PAPER

Eco-Friendly Synthesis of Stable Bismuth Nanoparticles Using Aegle marmelos Extract: Physicochemical Characterization and Antimicrobial Evaluation

Pooja Sankhla[1], YS Sarangdevot*[2] and Himanshu Paliwal[3]

[1]Research Scholar, Bhupal Nobles' College of Pharmacy, Bhupal Nobles' University, Udaipur, Rajasthan, 313001; India (PS)

[2]Professor, Faculty of Pharmacy, Bhupal Nobles' College of Pharmacy, Bhupal Nobles' University, Udaipur, Rajasthan, 313001; India. (YSS)

[3]Marwadi University Research Center, Faculty of Pharmacy, Marwadi University, Rajkot, 360003, Gujarat, India, Gujarat, India. (HP)

ABSTRACT

The green synthesis of metal nanoparticles is a promising alternative to traditional chemical methods that are environmentally hazardous and biologically incompatible. Here, bismuth nanoparticles (BiNPs) were synthesized using a hydroalcoholic Aegle marmelos leaf extract as a natural reducing, capping, and stabilizing agent. Various parameters of synthesis (volume of extract and temperature of reaction) were varied, keeping other conditions constant to obtain reproducible and controlled nanoparticle formation. The formation of BiNPs was confirmed by UV-Visible spectroscopy, showing characteristic absorption bands at 269-279 nm, and FTIR analysis, which showed the presence of plant-derived functional groups, such as hydroxyl and carbonyl moieties, which confirm their role in metal ion reduction and surface capping. The Nano sized BiNPs had hydrodynamic diameters between 34 and 61 nm and high negative surface charge values (-33.96 to -36.67 mV), which suggest good colloidal stability and effective surface capping. The efficient incorporation of bismuth was confirmed by inductively coupled plasma analysis, which revealed the highest metal content in batch S1. Concentration-dependent, broad-spectrum antimicrobial activity was demonstrated against selected bacterial and fungal strains, which was influenced by synthesis conditions and nanoparticle stability. In summary, this work presents a scalable and green approach for preparing BiNPs from Aegle marmelos with potential nano-enabled antimicrobial applications.

Graphical Abstract

Eco-Friendly Synthesis of Stable Bismuth Nanoparticles Using *Aegle marmelos* Extract: Physicochemical Characterization and Antimicrobial Evaluation

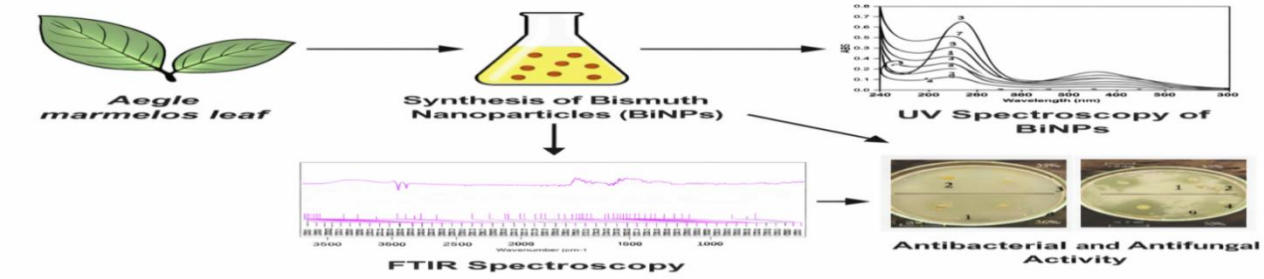

Keywords: ***Bismuth nanoparticles; Aegle marmelos; Green synthesis; Reproducible; Eco-friendly; Antimicrobial activity; Pharmaceutical nanotechnology.***

**Author for Correspondence: yuv_cog@rediffmail.com*

How to cite this article: Sankhla P, Sarangdevot YS, Paliwal H., Eco-Friendly Synthesis of Stable Bismuth Nanoparticles Using Aegle marmelos Extract: Physicochemical Characterization and Antimicrobial Evaluation .Int J Drug Deliv Technol. 2026;16(1s): 982-993; DOI: 10.25258/ijddt.16. 982-993
Source of support: Nil.
Conflict of interest: None

1. INTRODUCTION

Nanotechnology has emerged as a transformative field in material science and biomedical applications. Metal nanoparticles, especially those synthesized through green methods, are gaining prominence due to their biocompatibility, stability, and environmentally sustainable production [1, 2]. Among these, bismuth nanoparticles (BiNPs) offer unique properties including high atomic number make them good radio sensitizers (enhanced radiotherapy during cancer radiation therapy), low toxicity as compare to other heavy metals like lead, silver, mercury, gold etc., good renal clearance capacity (BiNP less than 6 mm naturally cleared through kidney) reduce long term bioaccumulation in body, collectively all make it safe and green heavy metal. It also possesses good antimicrobial & resistant breaking activity, making it suitable for biomedical imaging, drug delivery, and therapeutic applications [3, 4].

Conventional routes for synthesizing BiNPs utilize strong chemical reducing agents, organic solvents, high temperatures, and high energy consumption, producing toxic by-products and restricting their biomedical applications. Such methods are not consistent with green chemistry and are environmentally and biologically unsafe. To address these challenges, plant-mediated green synthesis has shown great potential, as phytochemicals in plant extracts can serve as reducing, capping, and stabilizing agents to produce safer and greener nanoparticles [5, 6].

Aegle marmelos (bael),a known medicinal plant with various bioactive phyto-constituents such as flavonoids, alkaloids, tannins, coumarins, terpenoids, and polyphenols, which have strong antioxidant and antimicrobial properties. They also reduce metal ions and provide surface capping and stabilization of nanoparticles, thus increasing the antimicrobial and biomedical potential of the resulting nanoparticles [7-9].

This research investigates the green synthesis of BiNPs using the most suitable *Aegle marmelos* leaf extract through the systematic and controlled variation of key synthesis parameters, such as the volume of extract and reaction temperature, and the impact on nanoparticle formation, yield, and colloidal stability. The physicochemical characterization of the synthesized BiNPs was conducted to evaluate surface chemistry, metal incorporation, and stability, followed by the evaluation of their antimicrobial potential against selected microbial strains.

2. MATERIALS AND METHODS

2.1. Plant Collection and Materials

Fresh Aegle marmelos leaves were collected from Udaipur, Rajasthan. *A. marmelos* was identified and confirmed by the B. N. College of Pharmacy, B. N. University, Udaipur, Rajasthan (BNU/Pharm./Auth./24-25/02), Udaipur, Rajasthan, India. Bismuth nitrate pentahydrate (Bi $(NO_3)_3 \cdot 5H_2O$ was purchased from Merck, India. All other reagents used were of analytical grade. The experiments were performed with sterile distilled water and deionized water.

2.2. Preparation of Plant Extract

Fresh leaves of '*Aegle marmelos'* were thoroughly washed, shade-dried, and finely powdered. The hydroalcoholic extract (70% ethanol) was prepared by macerating 10 g of the powdered plant material with 100 mL of 70% ethanol (ethanol: water, 7:3) at room temperature for 72 h with occasional shaking. The mixture was filtered through muslin cloth, followed by Whatman No. 1 filter paper. For nanoparticle synthesis, the dried hydroalcoholic extract was freshly reconstituted in distilled water to obtain the desired concentration and used as a natural reducing and stabilizing agent. The hydroalcoholic extract was phyto-chemically rich in flavonoids, phenolic, and tannins [10-12].

2.3. Phytochemical Screening

2.3.1. Total Phenolic Content (TPC)

TPC was determined using the Folin-Ciocalteu method with gallic acid as a standard. The reaction mixture containing Folin reagent, (Sodium Carbonate) Na_2CO_3, and the sample was incubated for 35 min in the dark, and absorbance was read at 725 nm.

2.3.2. Total Flavonoid Content (TFC)

TFC was measured by the aluminium chloride colorimetric method. The sample reacted with Sodium nitrite ($NaNO_3$), aluminium chloride ($AlCl_3$), and Sodium hydroxide (NaOH); absorbance was taken at 510 nm. Results expressed as mg/100 g of extract.

2.3.3. Total Tannin Content (TTC)

The estimation of TTC was carried out using the vanillin-HCl method. The sample mixed with vanillin-HCl reagent was incubated for 20 min, and absorbance was recorded at 500 nm.

2.3.4. Total Alkaloid Content (TAC)

Quantified by gravimetric analysis. Extracted with 10% acetic acid in ethanol, precipitated with ammonium hydroxide, dried and weighed. The results were indicated as % of dry weight.

2.3.5. Total Saponin Content (TSC)

It was evaluated by the foaming index method, wherein the extract solution was shaken and allowed to stand for 30 min; foam height was measured to determine saponin concentration. These phytochemical parameters were evaluated to establish a correlation between extract composition and nanoparticle formation efficiency [13, 14].

2.4. Preparation of Bismuth Nitrate Solution

Due to its high solubility and reactivity under aqueous conditions, $Bi(NO_3)_3 \cdot 5H_2O$ was used as the bismuth ion precursor. A 5 mM stock solution was prepared by weighing 2.43 g of $Bi(NO_3)_3 \cdot 5H_2O$ and dissolving it in 1000 mL of distilled water in a volumetric flask, which was stirred with a

magnetic stirrer until it was completely solubilized and homogeneous; the solution was then protected from light and used immediately for nanoparticle synthesis to minimize hydrolysis and instability of Bi ions [15].

2.5. pH Adjustment

The pH of the salt solution was adjusted to predetermined values (7.0, 9.0, and 12.0) using 0.1 N NaOH or 0.1 N HCl. Stirring was continued during pH adjustment to prevent local super saturation and premature precipitation of bismuth hydroxide.

2.6. Selection of Key Synthesis Parameters

From preliminary experiments, two synthesis parameters (plant extract volume and reaction temperature) were identified to significantly affect nanoparticle formation. The plant extract volumes were taken as 10, 25, and 50 mL, while the reaction temperatures were chosen as 50, 60, and 70 °C. These levels were selected to represent low, intermediate, and high conditions, enabling systematic evaluation of their influence on the behavior of nanoparticle formation.

2.7. Controlled Experimental Conditions

To isolate the specific effects of the volume of the plant extract and the reaction temperature on the formation of BiNPs, the concentration of $BiNO_3$ was kept constant at 5 mM, the volume of the precursor was kept constant at 50 mL, the stirring speed was kept at 500 rpm, and the reaction time was 2-3 h, so that the reaction environment was consistent across all synthesis runs and any variation was due to the synthesis parameters that were being investigated.

2.8. Experimental Formulation Layout for Green Synthesis of BiNPs

The plant extract and bismuth nitrate solution were mixed in different volumetric ratios comprising 10 mL, 25 mL, and 50 mL of extract, varying with a constant 50 mL $Bi(NO_3).5H_2O$. The mixtures were heated at 50°C, 60°C, and 70°C for 2-3 hours with continuous stirring at 500 rpm. A color change from pale yellow to dark brown/black indicated nanoparticle formation. Nine formulations (S1-S9) were prepared, which represent different combinations of extract volume and temperature with controlled pH conditions [16-18]. The formulation layout, extract volume, reaction temperature, and pH conditions are summarized in **Table 1**.

Table 1: Experimental formulation layout for synthesis of BiNPs

Formulation	Extract Volume (mL)	Temperature (°C)	pH
S1	25	50	12
S2	10	70	9
S3	50	50	7
S4	50	60	12
S5	25	70	9
S6	25	60	7
S7	10	50	12
S8	10	60	9
S9	50	70	12

Note: The pH of the bismuth nitrate solution was adjusted to pre-determined values (7.0, 9.0, and 12.0) by preliminary trials to avoid immediate precipitation of bismuth hydroxide and to ensure precursor stability. The pH was controlled as a pre-synthesis condition and was not considered as an independent design variable.

2.9. Purification of Nanoparticles

2.9.1. Centrifugation and Washing

The nanoparticle suspension after the synthesis reaction was centrifuged at 10,000 rpm for 20 min to pellet down the synthesized BiNPs from the reaction medium. The pellet was washed with a distilled water-ethanol mixture (2:1, v/v) to remove any unreacted precursors and loosely bound phytochemical residues, repeating the process 2-3 times to obtain a clear supernatant.

2.9.2. Sonication Method

After each wash, the nanoparticle pellet was re-suspended in distilled water by ultra-sonication at 40 kHz for 5 min to break up particle clumping and achieve uniform suspension. Sonication was used as an ancillary step to enhance nanoparticle homogeneity but was not used as a method of purification.

2.9.3. Drying and Storage

The purified nanoparticle suspension was lyophilized (freeze-dried) to obtain dry nanoparticle powder. Lyophilization was chosen to maintain particle stability and avoid aggregation during long-term storage. The dried nanoparticles were stored in sterile amber-colored vials under desiccated conditions until further characterization and biological evaluation.

2.10. Characterization of Synthesized BiNPs

After purification and drying, the synthesized BiNPs were subjected to physicochemical characterization to confirm nanoparticle formation, surface chemistry, stability, and crystallinity.

2.10.1. UV-Visible Spectroscopy

UV-Visible spectrophotometry was employed to confirm the formation of BiNPs and to compare the optical characteristics of the plant extract, bismuth nitrate solution, and synthesized BiNPs. Absorption spectra were recorded in the wavelength range of 200-800 nm using distilled water as a reference. The analysis was performed after completion of the synthesis process for each formulation.

2.10.2. Fourier Transform Infrared Spectroscopy (FTIR) analysis

FTIR spectra (4000-400 cm^{-1}) revealed the presence of -OH, C=O, and C-N groups, indicating that plant biomolecules were responsible for reducing and capping BiNPs. Comparison between the spectra of the extract and BiNPs showed peak shifts, confirming interaction with nanoparticle surfaces.

2.10.3. Zeta Potential and Particle Size Analysis

The colloidal stability and size distribution of the BiNP suspension were analyzed by particle size and zeta potential analysis using a Zetasizer Nano ZS (Malvern Instruments Ltd., Worcestershire, UK). Zeta potential was measured utilizing electrophoretic mobility and particle size from dynamic light scattering (DLS) at a fixed scattering angle of 173° (backscatter detection). For zeta potential measurement, the BiNP dispersion (1 mg/mL) was diluted with deionized water and loaded into a disposable folded capillary cell for analysis at room temperature (25 °C), and three runs per sample were performed to ensure reliable data. The zeta potential values more negative than -30 mV or more positive than +30 mV are indicative of adequate surface charge stability. Further, for determination of particle size and polydispersity index (PDI)

of BiNP, formulations were diluted with filtered deionized water (1:50–1:100), gently sonicated for 2–3 min, and analyzed by zetasizer at 25 ± 1 °C using disposable cuvettes. Measurements were performed in triplicate, and PDI values were recorded to evaluate size distribution uniformity.

2.10.4. Inductively Coupled Plasma (ICP) Analysis

The bismuth content was determined by elemental analysis using inductively coupled plasma optical emission spectrometry (ICP-OES). Approximately 0.5 g of dried sample was digested with concentrated nitric acid and hydrogen peroxide in a microwave digestion system at 180°C for 20 minutes. The digested sample was diluted to a constant volume with deionized water, filtered, and analyzed against calibration standards prepared in the same acid matrix. The bismuth concentration was calculated and reported as a weight percent of the total sample.

2.10.5. Microbial Evaluation

The antimicrobial activity of the synthesized nanoparticles was assessed using the agar well diffusion method using standard bacterial strains, including P. aeruginosa, E. coli (UPEC), and S. aureus (MRSA/MSSA), and fungal strains, such as A. niger and C. albicans. Bacterial cultures were grown on Mueller-Hinton agar, and fungal strains were grown on Sabouraud dextrose agar. Standardized microbial suspensions were prepared and standardized to turbidity (≈0.5 McFarland standard), and a uniform diameter (6 mm) wells were aseptically punched into the agar, and a fixed volume of nanoparticle suspensions (S1-S9) at predetermined concentrations (0.2 mg/mL) was added to each well. The standard antibiotics (Ciprofloxacin for Gram-negative bacteria, Vancomycin for Gram-positive bacteria, Amphotericin B for fungi) were employed as positive controls, and solvent or distilled water was used as a negative control. The incubation at 37 ± 2 °C for 24 h (bacteria) and 28 ± 2 °C for 48-72 h (fungi) was conducted, and the measurements of zones of inhibition around each well were measured in millimeters with a digital Vernier caliper. All experiments were carried out in triplicate, and the results were reported as mean ± standard deviation (SD)

2.11. Stability Study

The zeta potential stability of nanoparticle formulations (S1-S9) was determined over 15 days by dispersing samples in deionized water and sonication for 10 min to achieve a uniform suspension. It was followed by initial measurements on Day 0 using a zeta potential analyzer, and all readings were performed in triplicate to calculate mean ± SD. Samples were stored at ambient temperature in sealed vials and measured periodically on Days 1, 3, 5, 7, 10, and 15 under the same conditions, and changes in zeta potential over time were monitored to evaluate colloidal stability.

3. RESULTS AND DISCUSSION

3.1. Yield of Extracts

The percentage yield of extracts depended on the solvent system: the aqueous extraction yielded 11.2%, the ethanol and methanol extractions yielded 14.8% and 13.6%, respectively, and the hydroalcoholic (70% ethanol) extraction yielded 15.4%, which could be due to the solvent polarity and the solubility of the phytochemicals in the solvent. Hydroalcoholic solvents are known to extract a broader range of compounds due to their intermediate polarity, allowing better solubility of both hydrophilic and lipophilic phyto-constituents [19, 20].

3.2. Phytochemical Composition

3.2.1. Total Phenolic Content (TPC)

Highest in hydroalcoholic extract (98.3 ± 2.1 mg GAE/100 g), followed by methanol (92.5 ± 1.9), ethanol (87.4 ± 1.7), and aqueous (65.2 ± 1.5) extracts. Alcoholic solvents enhanced polyphenol solubility, correlating with strong bioactivity.

3.2.2. Total Flavonoid Content (TFC)

Hydroalcoholic extract showed the highest flavonoid content (74.6 ± 2.3 mg/100 g), followed by methanol (68.9 ± 1.8), ethanol (64.1 ± 2.0), and aqueous (45.3 ± 1.6) extracts. Indicates efficient extraction of bioactive flavonoids in alcohol-based solvents.

3.2.3. Total Tannin Content (TTC)

Hydroalcoholic extract exhibited maximum tannin content (56.3 ± 1.4 mg/100 g), followed by methanol (53.8 ± 1.2), ethanol (50.7 ± 1.5), and aqueous (37.1 ± 1.3) extracts. Tannins contribute to antimicrobial potential.

3.2.4. Total Alkaloid Content (TAC)

Alkaloid levels were highest in methanol (3.9%) and hydroalcoholic (3.7%) extracts, with moderate values in ethanol (3.4%) and lowest in aqueous (2.1%) extract. Alcoholic media favored alkaloid solubility.

3.2.5. Total Saponin Content (TSC)

Saponins were most abundant in aqueous extract (~2.5 cm foam height), followed by hydroalcoholic (~1.8 cm), ethanol (~1.2 cm), and methanol (~1.1 cm) extracts, reflecting their water solubility.

3.3. UV-Visible Spectroscopy

The UV-Visible absorption spectra of the synthesized BiNPs "showing six representative curves recorded during nanoparticle formation under identical experimental conditions", bismuth nitrate solution and plant extract are shown in **Fig. 1A, B, and C**. The plant extract exhibited characteristic absorption bands in the UV region, attributed to the presence of phytochemicals such as phenolic, terpenoids, and flavonoids. The solution of bismuth nitrate exhibited an absorption peak at 295 nm, which corresponded to the Bi^{3+} ionic species. BiNP samples prepared by green synthesis showed an absorption band or a distinctive SPR peak centered at about 275 nm, which has been reported as an indication of BiNPs formation, thus verifying the reduction of bismuth ions mediated by phytochemical constituents of the extract [21, 22].

The UV–Visible absorption spectra of the Extract, Bismuth salt and synthesized bismuth nanoparticles (BiNPs) were recorded in the range of 240–380 nm. As shown in the figure, a distinct surface plasmon resonance (SPR) peak was observed at approximately 275 nm, which is characteristic of BiNPs formation. The absorbance intensity varied across the nine samples (curves 1–9), indicating differences in concentration or extent of nanoparticle formation. [23, 24]. Among them, curve 1 exhibited the highest absorbance, while curve 6 showed the lowest.. The relatively broad nature of the absorption band is consistent with the reported optical

behavior of bismuth-based nanoparticles and may be associated with particle size distribution and surface capping by plant-derived biomolecules [25].

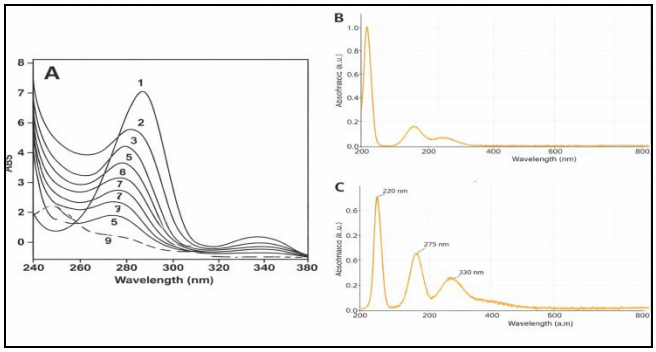

Fig. 1. UV Spectra of BiNPs (A), Bismuth Nitrate (B), and Aegle marmelos Extract (C).

3.4. FTIR analysis

FTIR analysis was carried out in the range of 4000-400 cm^{-1} to identify the functional groups involved in the reduction and stabilization (capping) of BiNPs. The FTIR spectrum of the plant extract exhibited characteristic peaks corresponding to major functional groups **(Fig. 2)**. A broad absorption band around 3300-3400 cm^{-1} is attributed to O-H stretching vibrations of alcohols or phenolic compounds. A sharp peak near 1640-1660 cm^{-1} corresponding to C=O stretching of carbonyl groups (likely from flavonoids or other polyphenols). A peak around 1380-1450 cm^{-1} is assigned to C-N stretching vibrations, suggesting the presence of amine or amide groups from proteins or alkaloids [26, 27].

In the FTIR spectrum of the synthesized BiNPs, these peaks were observed with slight shifts in position and changes in intensity, indicating interaction of the functional groups with the nanoparticle surface. Such peak shifts, particularly in the O-H and C=O regions, suggest the involvement of hydroxyl and carbonyl groups in metal ion reduction and subsequent surface capping through hydrogen bonding or coordination interactions.

Among all formulations, the optimized batch (S1) exhibited comparatively more pronounced peak shifts and higher peak intensities in the O-H and C=O regions, indicating stronger interaction and effective surface coverage of BiNPs by phytochemicals. In contrast, non-optimized formulations (S2-S9) showed relatively weaker or broader peaks, suggesting less efficient capping or partial interaction between biomolecules and nanoparticle surfaces. This comparative FTIR behavior supports the selection of S1 as the optimized formulation, correlating well with its superior stability and zeta potential results. Therefore, detailed FTIR interpretation was focused on the optimized formulation (S1), while spectra of other batches were included for comparative validation.

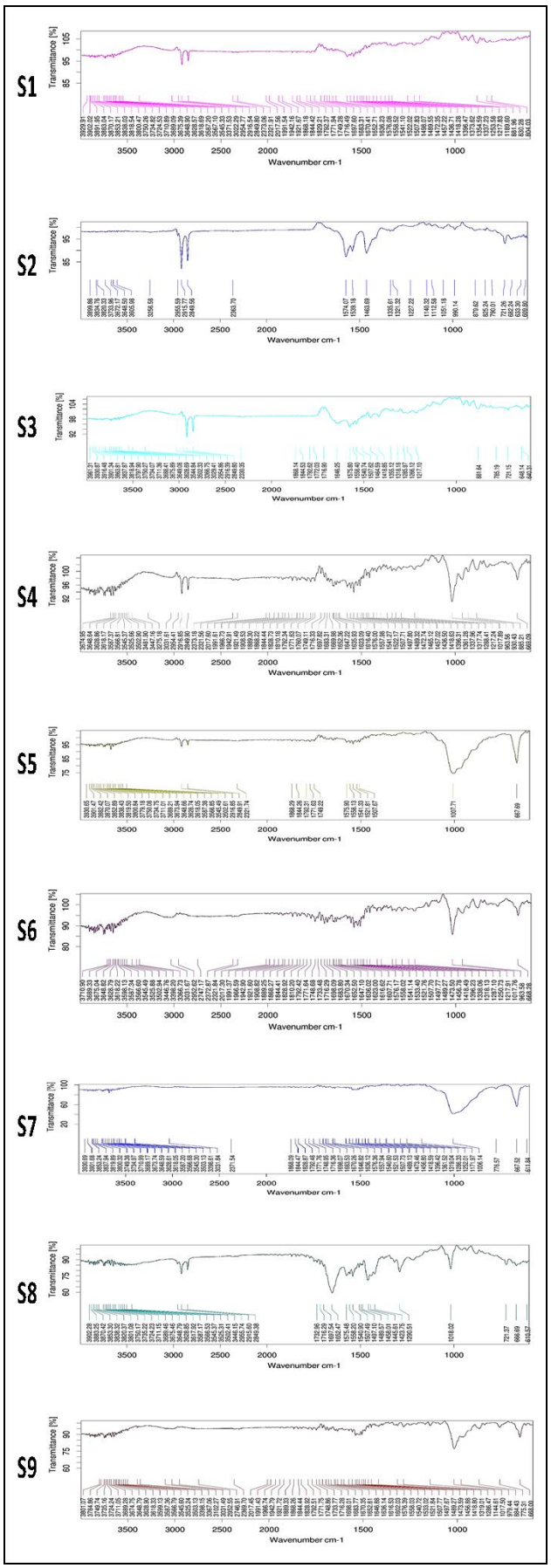

Fig. 2. FTIR spectra of different experiments (S1-S9).

3.5. Zeta Potential and Particle Size, Poly dispersity Index and Zeta Potential Analysis

The outcomes of zeta potential, particle size and PDI are summarized in **Table 2.** Formulations S1-S7 exhibited negative surface charges ranging from -33.96 to -36.67 mV, indicating good electrostatic stability and effective surface capping by plant-derived biomolecules. These formulations exhibited mean hydrodynamic diameters ranging from 34.12 ± 3.45 nm to 55.38 ± 3.44 nm, indicating successful formation of nano scale particles. The corresponding PDI values (0.182–0.271) suggested a relatively narrow size distribution and good dispersion uniformity, particularly for S1–S5. The gradual increase in particle size and PDI across these formulations reflects controlled modulation of synthesis parameters within the optimized design space.

In contrast, formulations S8 and S9 displayed comparatively larger particle sizes (58.62 ± 3.18 nm and 61.07 ± 3.95 nm, respectively) along with higher PDI values, indicating broader size distribution and partial aggregation due to the chosen synthesis conditions. Their zeta potential values (−28.34 ± 4.66 mV and −27.73 ± 5.86 mV) were lower in magnitude, suggesting comparatively reduced but still acceptable colloidal stability. The low surface charge and large particle size of these formulations could be attributed to the lack of availability or reduced activity of reducing and stabilizing phytochemicals at certain extract volumes or reaction temperatures [28, 29].

The surface charge on all formulations was consistently negative, which is mainly attributed to the adsorption of polyphenols, flavonoids, and other phenolic constituents from *Aegle marmelos* extract onto the nanoparticle surface, creating electrostatic repulsion and inhibiting agglomeration. Additionally, the standard deviations observed are comparable to the expected batch-to-batch variability observed in green synthesis processes, representing a practical robustness and reproducibility of the method rather than experimental inconsistency.

Table 2: Zeta potential, Particle size and PDI values obtained for different formulations

Formulations	Zeta Potential (mV)	Particle size (nm)	PDI
S1	**-34.65 ± 4.86**	**34.12 ± 3.45**	**0.182 ± 0.021**
S2	**-35.64 ± 7.48**	**38.47 ± 4.12**	**0.195 ± 0.018**
S3	**-34.74 ± 1.76**	**41.26 ± 3.68**	**0.207 ± 0.024**
S4	**-34.37 ± 3.13**	**44.83 ± 3.21**	**0.221 ± 0.019**
S5	**-33.96 ± 2.98**	**48.95 ± 4.87**	**0.238 ± 0.027**
S6	**-36.67 ± 4.56**	**52.14 ± 4.02**	**0.254 ± 0.022**
S7	**-35.45 ± 5.45**	**55.38 ± 3.44**	**0.271 ± 0.025**
S8	**-28.34 ± 4.66**	**58.62 ± 3.18**	**0.318 ± 0.031**
S9	**-27.73 ± 5.86**	**61.07 ± 3.95**	**0.346 ± 0.029**

3.6. ICP Analysis of BiNPs

The Bi content in the synthesized nanoparticles (S1-S9) was quantified using inductively coupled plasma (ICP) analysis as weight percentage (wt%), as shown in **Fig. 3**. The Bi content of the samples slightly varied among the formulations; samples S1, S3, and S2 had the highest Bi content (close to 99-100 wt%), which indicates that the metal was incorporated efficiently during nanoparticle synthesis. Samples S4, S5, S6, and S7 had slightly lower Bi content (~94-97 wt%), while S8 and S9 had the lowest values (around 86-88 wt%).

These fluctuations in Bi content can be attributed to differences in reaction efficiency, capping agent interaction, or minor aggregation during synthesis, and the high Bi content of most samples suggests successful formation of BiNPs with minimal loss during preparation. The slightly lower Bi content in S8 and S9 may suggest partial surface oxidation or incomplete reduction of bismuth precursors in these formulations. The ICP results show that the green synthesis method used produces nanoparticles with consistently high Bi content, which makes them ideal for further characterization and application [30, 31] **(Fig. 3)**.

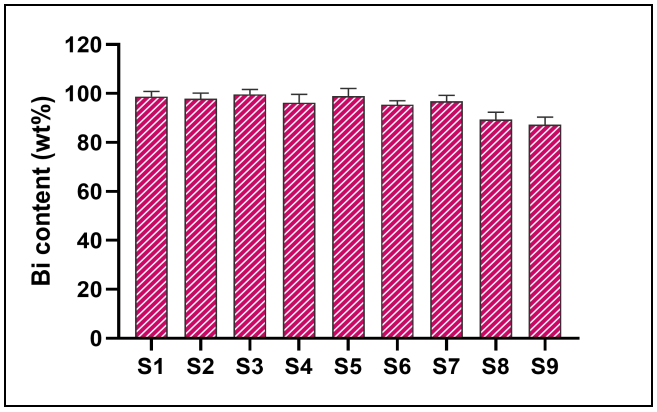

Fig. 3. Simulated ICP results of different S1-S9 samples of BiNPs.

3.7. Antimicrobial Activity of Nanoparticles

The antimicrobial activity of the synthesized nanoparticles was tested against a panel of bacterial and fungal pathogens, including *Pseudomonas aeruginosa*, *Escherichia coli* (UPEC), *Staphylococcus aureus* (MRSA/MSSA), *Aspergillus niger*, and *Candida albicans*. The results are reported as zones of inhibition (mm, mean ± SD) and are presented in **Table 3**. The results were compared to standard antibiotics: Ciprofloxacin for Gram-negative bacteria, Vancomycin for Gram-positive bacteria, and Amphotericin B for fungi.

Table 3: Microbial Evaluation of BiNPs(Zone of Inhibition in mm)

Microorganism	Type	S1	S2	S3	S4	S5	S6	S7	S8	S9	Standard Antibiotic (Control)
Pseudomonas aeruginosa	Gram-negative Bacteria	11 ± 0.4	8 ± 0.3	13 ± 0.5	12 ± 0.4	12 ± 0.3	14 ± 0.4	13 ± 0.5	14 ± 0.3	11 ± 0.4	Ciprofloxacin (28 ± 0.5)
Escherichia coli (UPEC)	Gram-negative Bacteria	12 ± 0.3	--	--	11 ± 0.3	7 ± 0.2	6 ± 0.5	8 ± 0.3	8 ± 0.4	7 ± 0.4	Ciprofloxacin (27 ± 0.6)
Staphylococcus aureus (MRSA/MSSA)	Gram-positive Bacteria	19 ± 0.3	13 ± 0.3	4 ± 0.4	--	3 ± 0.5	--	--	--	--	Vancomycin (30 ± 0.6)
Aspergillus Niger (Resistant strain)	Fungi	9 ± 0.4	10 ± 0.3	11 ± 0.3	13 ± 0.4	--	--	--	--	--	Amphotericin B (29 ± 0.4)
Candida albicans (Resistant strain)	Fungi	7 ± 0.4	--	--	--	7 ± 0.3	18 ± 0.4	--	--	--	Amphotericin B (32 ± 0.4)
Escherichia coli (EPEC)	Gram-negative Bacteria	8 ± 0.5	7 ± 0.4	7 ± 0.5	6 ± 0.1	4 ± 0.1	4 ± 0.8	3 ± 0.8	4 ± 0.4	3 ± 0.5	Azithromycin (25 ± 0.5)
Staphylococcus epidermidis	Gram-positive Bacteria	9 ± 0.6	6 ± 0.5	7 ± 0.4	7 ± 0.3	6 ± 0.2	5 ± 0.3	5 ± 0.4	6 ± 0.3	5 ± 0.3	Rifampin (26 ± 0.5)
Aspergillus flavus (Resistant strain)	Fungi	9 ± 0.3	8 ± 0.8	8 ± 0.6	7 ± 0.4	6 ± 0.8	6 ± 0.1	4 ± 0.3	3 ± 0.6	3 ± 0.1	Amphotericin B (30 ± 0.3)
Candida glabrata (Resistant strain)	Fungi	10 ± 0.1	8 ± 0.3	7 ± 0.8	8 ± 0.6	7 ± 0.4	8 ± 0.7	8 ± 0.1	6 ± 0.6	7 ± 0.7	Amphotericin B (28 ± 0.6)

3.7.1. Antibacterial Activity

The synthesized nanoparticles showed varying inhibition against *Pseudomonas aeruginosa* and *Escherichia coli* (UPEC). *P. aeruginosa* showed 14 ± 0.4 mm (maximum) with S6 and S8, 13 ± 0.5 mm with S3 and S7, moderate activity with S1 (11 ± 0.4 mm) and S4 (12 ± 0.4 mm), S2 and S9, and positive control Ciprofloxacin 28 ± 0.5 mm, which confirms the validity of the assay. This moderate activity indicates that the nanoparticles penetrated the outer membrane of *P. aeruginosa*, a notoriously resistant Gram-negative bacterium. The differences in inhibition for the samples suggest that antibacterial potency could be influenced by particle size, surface charge, or capping biomolecules present on the surface of the nanoparticles, possibly derived from plant extracts [32]. *E. coli* (UPEC) was less sensitive to most nanoparticle samples, with S1 having the greatest inhibition (12 ± 0.3 mm) and S5-S9 having the lowest inhibition (6-8 mm), which could be a result of the thick lipopolysaccharide layer of *E. coli* that restricts nanoparticle penetration or due to suboptimal binding affinity of the nanoparticles with bacterial cell surface components. The trend in activity suggests that certain nanoparticle compositions or surface modifications (e.g., in S1) are critical for bactericidal activity [33].

The synthesized nanoparticles exhibited pronounced inhibitory activity against Staphylococcus aureus (MRSA/MSSA). Among all tested samples, S1 produced the largest inhibition zone (19 ± 0.3 mm), followed by S2 (13 ± 0.3 mm). Samples S3-S9 showed negligible to no activity. Vancomycin, the standard, produced an inhibition zone of 30 ± 0.6 mm. The higher susceptibility of S. aureus can be attributed to the simpler peptidoglycan layer of Gram-positive bacteria, which allows better nanoparticle interaction and disruption of the cell wall. The presence of bioactive phyto constituents on the nanoparticle surface may have further enhanced membrane permeability and oxidative stress within

bacterial cells, leading to cell lysis [34].

3.7.2. Antifungal Activity

The nanoparticles also demonstrated notable antifungal activity, particularly against Aspergillus niger and Candida albicans. For A. niger, the inhibition zone increased progressively from S1 (9 ± 0.4 mm) to S4 (13 ± 0.4 mm), indicating concentration-dependent efficacy. No inhibition was observed with samples beyond S4, indicating that moderate nanoparticle concentrations may be more effective for active antifungal components. For the control Amphotericin B, 29 ± 0.4 mm inhibition was observed and S6 showed remarkable inhibition (18 ± 0.4 mm) against Candida albicans, and S1 and S5 showed only weak zones (7 ± 0.3-0.4 mm). This increase in activity could be due to the optimal size-to-surface ratio, which leads to better adhesion and disruption of fungal cell membranes. The mechanism of antifungal activity probably involves the generation of reactive oxygen species (ROS) and membrane destabilization due to metal ions released from nanoparticles [35, 36].

3.7.3. Comparative Evaluation and Mechanistic Insights

The antimicrobial activity followed the general trend:
S. *aureus* > *P. aeruginosa* > *A. niger* > *C. albicans* > *E. coli.*
This implies that Gram-positive bacteria were more sensitive to nanoparticle exposure than Gram-negative strains, possibly because of the differences in their cell envelopes. The antifungal results indicate possible use against resistant fungal strains such as *Candida albicans* and *Aspergillus niger*. Variation in samples S1-S9 could be due to variations in nanoparticle size, concentration, and capping phytochemicals from the natural extract used during synthesis. These smaller particles have increased surface energy, which allows them to interact with microbial membranes, causing leakage of intracellular contents and cell death [37]. The nanoparticles synthesized showed broad-spectrum antimicrobial activity and were effective against *Staphylococcus aureus* and moderately active against fungal pathogens. The results (Zone of inhibition assay as a preliminary screening tool) suggest that green-synthesized nanoparticles may be potential antimicrobials, particularly against antibiotic-resistant bacteria and pathogenic fungi. Additional studies with mechanistic assays (MIC determination and ROS generation, protein leakage) are necessary to determine the mode of action and optimize formulation parameters [38, 39].

3.8. Stability Studies

The zeta potential stability study over 15 days showed a gradual decrease of negative surface charge for all BiNPs samples (S1-S9); samples S1-S7 still had relatively high negative zeta potential values (-31 to -36 mV) at day 15, suggesting good colloidal stability and low aggregation over time. In contrast, S8 and S9 showed a more pronounced reduction in zeta potential (-22.74 mV and -21.73 mV, respectively) by day 15, suggesting lower electrostatic stabilization and a higher tendency for particle aggregation. Overall, the data indicate that formulations S1-S7 are more stable, whereas S8 and S9 may require additional stabilization strategies to maintain nanoparticle dispersion (Table 4).

Table 4. Zeta potential results during the stability study conducted for 15 days

Sample	Day 0	Day 1	Day 3	Day 5	Day 7	Day 10	Day 15
S1	-34.65 ± 4.86	-34.45 ± 4.93	-34.05 ± 5.05	-33.65 ± 5.19	-33.25 ± 5.34	-32.65 ± 5.57	-31.65 ± 6.05
S2	-35.64 ± 7.48	-35.44 ± 7.61	-35.04 ± 7.82	-34.64 ± 8.05	-34.24 ± 8.29	-33.64 ± 8.70	-32.64 ± 9.39
S3	-34.74 ± 1.76	-34.54 ± 1.78	-34.14 ± 1.83	-33.74 ± 1.88	-33.34 ± 1.93	-32.74 ± 2.01	-31.74 ± 2.13
S4	-34.37 ± 3.13	-34.17 ± 3.19	-33.77 ± 3.29	-33.37 ± 3.39	-32.97 ± 3.49	-32.37 ± 3.63	-31.37 ± 3.85
S5	-33.96 ± 2.98	-33.76 ± 3.03	-33.36 ± 3.13	-32.96 ± 3.23	-32.56 ± 3.33	-31.96 ± 3.47	-30.96 ± 3.68
S6	-36.67 ± 4.56	-36.47 ± 4.63	-36.07 ± 4.75	-35.67 ± 4.88	-35.27 ± 5.01	-34.67 ± 5.18	-33.67 ± 5.46
S7	-35.45 ± 5.45	-35.25 ± 5.54	-34.85 ± 5.67	-34.45 ± 5.81	-34.05 ± 5.95	-33.45 ± 6.16	-32.45 ± 6.51
S8	-28.34 ± 4.66	-28.02 ± 4.83	-27.38 ± 5.14	-26.74 ± 5.45	-26.10 ± 5.77	-24.82 ± 6.38	-22.74 ± 7.31
S9	-27.73 ± 5.86	-27.40 ± 6.04	-26.73 ± 6.36	-26.07 ± 6.69	-25.40 ± 7.03	-24.07 ± 7.67	-21.73 ± 8.79

4. CONCLUSIONS

This study established a green and reproducible method for the synthesis of BiNPs using hydroalcoholic Aegle marmelos leaf extract as a natural reducing and stabilizing agent. A systematic controlled experimental design allowed for the characterization of a stable synthesis design space (S1-S7) in which key quality attributes such as surface charge, particle size, stability, and reproducibility were maintained within acceptable limits. The formation of nanoparticles was confirmed by UV-Visible spectroscopy, which showed a characteristic absorption band in the range of 269-279 nm, and the involvement of phytochemical functional groups, hydroxyl and carbonyl moieties, in BiNP reduction and surface capping was confirmed by FTIR analysis. The zeta potential and particle size analysis revealed nano sized BiNPs with high negative surface charge, demonstrating reduced

aggregation tendency and sustained colloidal stability. The 15-day stability study demonstrated that these formulations retained colloidal behavior, while batches outside the design space exhibited lower stability. While some formulations displayed enhanced antimicrobial activity against specific microbial strains, antimicrobial performance alone was not used as the sole optimization parameter. S1 was selected as a representative optimized batch based on an integrated assessment of physicochemical stability, surface chemistry, metal content, reproducibility, and consistent broad-spectrum antimicrobial response, demonstrating robustness and reliability rather than optimization based on a single biological endpoint. In conclusion, our results show that BiNPs with controllable surface charge, effective phytochemical capping, and high metal incorporation could be reproducibly prepared by plant-mediated green synthesis, and the integrated evaluation of physicochemical stability, smallest particle size (34.12 ± 3.45 nm), lowest PDI (0.182 ± 0.021), strong negative surface charge (−34.65 ± 4.86 mV) , ICP-confirmed bismuth content and antimicrobial consistency support the selection of S1 as a representative optimized formulation and provide a strong basis for further advanced physicochemical characterization of BiNPs, such as XRD and SEM/TEM to confirm crystalline nature, particle size, shape, and morphology. Additionally, minimum inhibitory concentration (MIC) analysis may be performed to quantitatively validate antimicrobial potency and formulation consistency. The correlation of physicochemical attributes with MIC outcomes will help assess the synergistic effects of BiNPs and plant-derived phytochemicals and provide insight into their probable antimicrobial mode of action.

5. DATA AVAILABILITY:

The datasets generated and/or analysed during the current study are available from the corresponding author upon reasonable request.

6. DECLARATION OF COMPETING INTEREST

The authors declare that they have no known competing financial interests or personal relationships that could have appeared to influence the work reported in this paper.

7. ACKNOWLEDGMENTS

The authors would like to thank Faculty of Pharmacy, B.N. University, Rajasthan, India, and Ozone Test House for their support and providing instrumental facilities.

8. REFERENCES

1. S. Dubale, D. Kebebe, A. Zeynudin, N. Abdissa, S. Suleman, Phytochemical Screening and Antimicrobial Activity Evaluation of Selected Medicinal Plants in Ethiopia, J. Exp. Pharmacol. 15 (2023) 51-62, https://doi.org/10.2147/jep.S379805.
2. R. Gonzalez-Pastor, S.E. Carrera-Pacheco, J. Zúñiga-Miranda, C. Rodríguez-Pólit, A. Mayorga-Ramos, L.P. Guamán, C. Barba-Ostria, Current Landscape of Methods to Evaluate Antimicrobial Activity of Natural Extracts, Molecules 28 (3) (2023) 1068, https://doi.org/10.3390/molecules28031068.
3. C. Mallikarjunaswamy, S. Pramila, G. Nagaraju, R. Ramu, V.L. Ranganatha, Green synthesis and evaluation of antiangiogenic, photocatalytic, and electrochemical activities of BiVO4 nanoparticles, Journal of Materials Science: Materials in Electronics 32 (10) (2021) 14028-14046, https://doi.org/10.1007/s10854-021-05980-w.
4. N. Vaou, E. Stavropoulou, C. Voidarou, Z. Tsakris, G. Rozos, C. Tsigalou, E. Bezirtzoglou, Interactions between Medical Plant-Derived Bioactive Compounds: Focus on Antimicrobial Combination Effects, Journal 11 (8) (2022) 1014, https://doi.org/10.3390/antibiotics11081014.
5. C. Pandit, A. Roy, S. Ghotekar, A. Khusro, M.N. Islam, T.B. Emran, S.E. Lam, M.U. Khandaker, D.A. Bradley, Biological agents for synthesis of nanoparticles and their applications, Journal of King Saud University - Science 34 (3) (2022) 101869, https://doi.org/10.1016/j.jksus.2022.101869.
6. X. Jiang, S. Khan, A. Dykes, E. Stulz, X. Zhang, Biogenic Synthesis of Silver Nanoparticles and Their Diverse Biomedical Applications, Journal 30 (15) (2025) 3104, https://doi.org/10.3390/molecules30153104.
7. S. Monika, M. Thirumal, P.R. Kumar, Phytochemical and Biological Review of Aegle Marmelos Linn, Future Science OA 9 (3) (2023) FSO849, https://doi.org/10.2144/fsoa-2022-0068.
8. F. Kousar, A. Khanem, I. Ullah, F. Younas, Phytochemical analysis and synergistic antimicrobial potential of extracts from Carica papaya and Beta vulgaris, Kuwait Journal of Science 50 (3) (2023) 307-312, https://doi.org/10.1016/j.kjs.2023.05.010.
9. H.H. Shahin, M. Baroudi, F. Dabboussi, B. Ismail, R. Salma, M. Osman, K. El Omari, Synergistic Antibacterial Effects of Plant Extracts and Essential Oils Against Drug-Resistant Bacteria of Clinical Interest, Journal 14 (4) (2025) 348, https://doi.org/10.3390/pathogens14040348.
10. M.A. Dheyab, N. Oladzadabbasabadi, A.A. Aziz, P.M. Khaniabadi, M.T.S. Al-ouqaili, M.S. Jameel, F.S. Braim, B. Mehrdel, M. Ghasemlou, Recent advances of plant-mediated metal nanoparticles: Synthesis, properties, and emerging applications for wastewater treatment, Journal of Environmental Chemical Engineering 12 (2) (2024) 112345, https://doi.org/10.1016/j.jece.2024.112345.
11. M. Prakash, H.P. Kavitha, S. Abinaya, J.P. Vennila, D. Lohita, Green synthesis of bismuth based nanoparticles and its applications - A review, Sustainable Chemistry and Pharmacy 25 (2022) 100547, https://doi.org/10.1016/j.scp.2021.100547.
12. A.S. Dousari, S.S. Hosseininasab, M.R. Akbarizadeh, M. Naderifar, N. Satarzadeh, Mentha pulegium as a source of green synthesis of nanoparticles with antibacterial, antifungal, anticancer, and antioxidant applications, Scientia Horticulturae 320 (2023) 112215, https://doi.org/10.1016/j.scienta.2023.112215.

13. A. Subhan, A.H.I. Mourad, S. Das. *Pulsed Laser Synthesis of Bi-Metallic Nanoparticles for Biomedical Applications: A Review*. in *2022 Advances in Science and Engineering Technology International Conferences (ASET)*. 2022.
14. B. Mughal, S.Z. Zaidi, X. Zhang, S.U. Hassan, Biogenic Nanoparticles: Synthesis, Characterisation and Applications, Journal 11 (6) (2021) 2598, https://doi.org/10.3390/app11062598.
15. A. Haleem, M. Javaid, R.P. Singh, S. Rab, R. Suman, Applications of nanotechnology in medical field: a brief review, Global Health Journal 7 (2) (2023) 70-77, https://doi.org/10.1016/j.glohj.2023.02.008.
16. M. El kadiri, T. El Assimi, P. Thébault, A. El Meziane, S. Royer, A. El Kadib, G. Gouhier, M. Lahcini, Bismuth Nanoparticles Supported on Biobased Chitosan as Sustainable Catalysts for the Selective Hydrogenation of Nitroarenes, ACS Applied Nano Materials 6 (5) (2023) 4017-4027, https://doi.org/10.1021/acsanm.3c00333.
17. G. Hallot, V. Cagan, S. Laurent, C. Gomez, M. Port, A Greener Chemistry Process Using Microwaves in Continuous Flow to Synthesize Metallic Bismuth Nanoparticles, ACS Sustainable Chemistry & Engineering 9 (28) (2021) 9177-9187, https://doi.org/10.1021/acssuschemeng.1c00396.
18. R.K. Selvakesavan, G. Franklin, Prospective Application of Nanoparticles Green Synthesized Using Medicinal Plant Extracts as Novel Nanomedicines, Nanotechnol Sci Appl 14 (2021) 179-195, https://doi.org/10.2147/nsa.S333467.
19. J.-E. Lee, J.T. Jayakody, J.-I. Kim, J.-W. Jeong, K.-M. Choi, T.-S. Kim, C. Seo, I. Azimi, J. Hyun, B. Ryu, The Influence of Solvent Choice on the Extraction of Bioactive Compounds from Asteraceae: A Comparative Review, Journal 13 (19) (2024) 3151, https://doi.org/10.3390/foods13193151.
20. E. Gil-Martín, T. Forbes-Hernández, A. Romero, D. Cianciosi, F. Giampieri, M. Battino, Influence of the extraction method on the recovery of bioactive phenolic compounds from food industry by-products, Food Chem. 378 (2022) 131918, https://doi.org/10.1016/j.foodchem.2021.131918.
21. N. Motakef-Kazemi, M. Yaqoubi, Green Synthesis and Characterization of Bismuth Oxide Nanoparticle Using Mentha Pulegium Extract, Iranian Journal of Pharmaceutical Research 19 (2) (2020) 70-79, https://doi.org/10.22037/ijpr.2019.15578.13190.
22. P. Moorthy, H.P. Kavitha, Comparative Evaluation of Bioefficiency and Photocatalytic Activity of Green Synthesized Bismuth Oxide Nanoparticles Using Three Different Leaf Extracts, ACS Omega 8 (16) (2023) 14752-14765, https://doi.org/10.1021/acsomega.3c00792.
23. O. Velgosova, L. Mačák, M. Lisnichuk, P. Varga, Influence of pH and Temperature on the Synthesis and Stability of Biologically Synthesized AgNPs, Journal 6 (4) (2025) 22, https://doi.org/10.3390/applnano6040022.
24. G. Arroyo, Y. Angulo, B. Naranjo, F. Toscano, M.T. Arias, A. Debut, C. Reinoso, C. Stael, J. Soria, A. Izquierdo, Green synthesis of antioxidant and low-toxicity gold and silver nanoparticles using floral extracts, OpenNano 26 (2025) 100258, https://doi.org/10.1016/j.onano.2025.100258.
25. M.-A. Shahbazi, L. Faghfouri, M.P.A. Ferreira, P. Figueiredo, H. Maleki, F. Sefat, J. Hirvonen, H.A. Santos, The versatile biomedical applications of bismuth-based nanoparticles and composites: therapeutic, diagnostic, biosensing, and regenerative properties, Chem. Soc. Rev. 49 (4) (2020) 1253-1321, https://doi.org/10.1039/C9CS00283A.
26. M. Farahani, A. Jalali, S. Moghadasi, M. Rezaei, R. Khodadadi, Investigating the Impact of Bismuth Oxide Nanoparticles on Dazl Gene Expression and Spermatogenesis Indices in Male Mice, Biol. Trace Elem. Res. 203 (10) (2025) 5245-5261, https://doi.org/10.1007/s12011-025-04554-9.
27. C. Manoharan, R. Rammohan, R. Subramanian, V. Umashanker, Synthesis of α-Bismuth oxide nanoparticles, spectral characterization and their photocatalytic activity, Inorganic and Nano-Metal Chemistry 53 (2) (2023) 113-121, https://doi.org/10.1080/24701556.2021.1986526.
28. A.F. Burlec, A. Corciova, M. Boev, D. Batir-Marin, C. Mircea, O. Cioanca, G. Danila, M. Danila, A.F. Bucur, M. Hancianu, Current Overview of Metal Nanoparticles' Synthesis, Characterization, and Biomedical Applications, with a Focus on Silver and Gold Nanoparticles, Journal 16 (10) (2023) 1410, https://doi.org/10.3390/ph16101410.
29. M. Shahalaei, A.K. Azad, W.M.A.W. Sulaiman, A. Derakhshani, E.B. Mofakham, M. Mallandrich, V. Kumarasamy, V. Subramaniyan, A review of metallic nanoparticles: present issues and prospects focused on the preparation methods, characterization techniques, and their theranostic applications, Frontiers in Chemistry 12 (2024) https://doi.org/10.3389/fchem.2024.1398979.
30. M. Mahiuddin, B. Ochiai, Comprehensive Study on Lemon Juice-Based Green Synthesis and Catalytic Activity of Bismuth Nanoparticles, ACS Omega 7 (40) (2022) 35626-35634, https://doi.org/10.1021/acsomega.2c03416.
31. M.A. Rahman, M.A. Rahman, M.A. Rabbi, M. Rana, M.R. Karim, M.A. Jalil Miah, H. Ahmad, Highly efficient recyclable bismuth nanocatalysts fabricated using a facile one-step aqueous method for faster reduction of azo dye contaminants, RSC Advances 14 (34) (2024) 24447-24461, https://doi.org/10.1039/D4RA04625K.
32. D. de Lacerda Coriolano, J.B. de Souza, E.V. Bueno, S.M.d.F.R.d.S. Medeiros, I.D.L. Cavalcanti, I.M.F. Cavalcanti, Antibacterial and antibiofilm potential of silver nanoparticles against antibiotic-sensitive and multidrug-resistant Pseudomonas aeruginosa strains,

Braz J Microbiol 52 (1) (2021) 267-278, https://doi.org/10.1007/s42770-020-00406-x.

33. P.R. More, S. Pandit, A.D. Filippis, G. Franci, I. Mijakovic, M. Galdiero, Silver Nanoparticles: Bactericidal and Mechanistic Approach against Drug Resistant Pathogens, Journal 11 (2) (2023) 369, https://doi.org/10.3390/microorganisms11020369.
34. H.O. Khalifa, A. Oreiby, T. Mohammed, M.A.A. Abdelhamid, E.N. Sholkamy, H. Hashem, R.M. Fereig, Silver nanoparticles as next-generation antimicrobial agents: mechanisms, challenges, and innovations against multidrug-resistant bacteria, Frontiers in Cellular and Infection Microbiology 15 (2025) https://doi.org/10.3389/fcimb.2025.1599113.
35. H.F.Z. Touil, K. Boucherit, Z. Boucherit-Otmani, G. Kohder, M. Madkour, S.S.M. Soliman, Optimum Inhibition of Amphotericin-B-Resistant Candida albicans Strain in Single- and Mixed-Species Biofilms by Candida and Non-Candida Terpenoids, Journal 10 (2) (2020) 342, https://doi.org/10.3390/biom10020342.
36. E.I. Muresan, A. Pui, C. Cernatescu, R. Cimpoesu, C.E. Horhogea, B. Istrate, C.M. Rîmbu, Green Synthesis of Nanoparticles Containing Zinc Complexes and Their Incorporation in Topical Creams with Antimicrobial Properties, Journal 14 (11) (2024) 4612, https://doi.org/10.3390/app14114612.
37. E. Abada, A. Mashraqi, Y. Modafer, M.A. Al Abboud, A. El-Shabasy, Review green synthesis of silver nanoparticles by using plant extracts and their antimicrobial activity, Saudi J. Biol. Sci. 31 (1) (2024) 103877, https://doi.org/10.1016/j.sjbs.2023.103877.
38. S. Dybkova, K. Terpilowski, O. Goncharuk, M. Dybkov, L. Rieznichenko, O. Liutko, K. Vitrak, T. Gruzina, K. Szewczuk-Karpisz, Antimicrobial Efficiency of 'Green' Silver Nanoparticles Against Plant and Human Pathogens for Environmental Sanitation, Journal 18 (21) (2025) 4952, https://doi.org/10.3390/ma18214952.
39. M. Gupta, R.S. Tomar, S. Kaushik, R.K. Mishra, D. Sharma, Effective Antimicrobial Activity of Green ZnO Nano Particles of Catharanthus roseus, Front. Microbiol. 9 (2018) https://doi.org/10.3389/fmicb.2018.02030.